Time delay signature concealment of chaotic semiconductor laser subject to nonlinear feedback

Chenpeng Xue (薛琛鹏), Ning Jiang (江 宁)*, Yunxin Lv (吕韵欣), and Kun Qiu (邱 昆)

Key Laboratory of Optical Fiber Sensing and Communications, Ministry of Education, University of Electronic Science and Technology of China, Chengdu 611731, China

**Corresponding author: uestc_nj@uestc.edu.cn*

Received May 24, 2016; accepted July 19, 2016; posted online August 9, 2016

An external-cavity semiconductor laser with nonlinear optical feedback to generate broadband chaos with time delay signature (TDS) suppression is investigated. The system is composed of three semiconductor lasers, one of which is regarded as the chaos generator, while the other two play a role of a built-in nonlinear modulator in the external cavity of the generator. The results show that by properly setting the feedback strength and time delay of the first semiconductor laser in the nonlinear modulator, the TDS embedded in the intensity and phase time-series of the chaos can be effectively concealed in a wide range of frequency detuning.

OCIS codes: 140.1540, 140.5960, 190.3100.

doi: 10.3788/COL201614.091404.

Chaos generated by the external-cavity semiconductor laser (ECSL) with delayed optical feedback has drawn considerable attention for its potential applications in many fields, such as secure communication[1–4], fast random bit generators (RBGs)[5–8], chaotic lidar/radar[9,10], and optical time domain reflectometer (OTDR)[11]. Although the ECSL with a delayed optical feedback can easily generate broadband and high complexity chaotic signals, the chaos usually also shows an obvious time delay signature (TDS), which is undesirable in some of the applications. For chaos-based secure communication, the security is majorly dependent on the difficulty of the identification of the emitter parameters, especially the time delay, which can provide one of the possible clues for the attackers to reconstruct the chaotic carrier[12]. For the RBGs, the recurrence feature of the physical source induced by the TDS would reduce the randomness of the RBGs[5,6].

On one hand, technologies, such as power spectrum analysis, auto-correlation function (ACF), delayed mutual information (DMI), and permutation entropy (PE), have been widely used to observe the TDS embedded in the chaotic signal[13–15]. Besides, it is also reported that the TDS can be successfully retrieved by computing the same quantifiers from the phase time-series[16]. On the other hand, a lot of schemes for the purpose of TDS concealment are also reported[17–26]. For instance, Wu *et al.* found that the semiconductor laser (SL) that is subject to double delayed feedback loops can effectively suppress the TDS in the chaotic signal[18]. Nguimdo *et al.* predicted that the TDS could be lost simultaneously in the intensity and phase dynamics of semiconductor ring lasers with cross optical feedback[19]. Li *et al.* reported that fiber Bragg grating feedback can be used to suppress the TDS[20]. All of these studies motivate further investigations on the TDS concealment of chaotic SLs for its potential applications in the physical secure communications and RBGs.

Very recently, the scheme that a ring of three unidirectionally coupled SLs can be used to suppress the TDS in both the intensity and phase space of chaos has been numerically demonstrated[25]. However, the physical principles of TDS concealment in the system are not provided and the TDS concealment can be further investigated. In this Letter, we proposed an advanced system in which a ring of three unidirectionally coupled SLs with optical feedback are adopted to generate chaos with the TDS eliminated. The ACF and DMI of the intensity and phase time-series are calculated to identify the TDS in the chaotic signal. According to our results, by making use of the feedback term in SL2, the TDS embedded in the intensity and phase time-series of chaos in SL1 can be effectively suppressed.

The structure of the system composed of three SLs is depicted in Fig. 1. In the system, SL1 is regarded as the chaos signal source, its output is unidirectionally injected into SL2; then, the output of SL2 is unidirectionally injected into SL3; finally, the output of SL3 is unidirectionally injected back into SL1. Here, SL2 and SL3 are equivalent to a nonlinear modulator which can suppress the TDS of the chaotic signal induced by the fixed period stemming from the fixed-length external cavity.

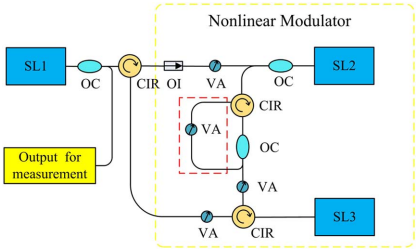

Fig. 1. Structure of the proposed laser ring. CIR, optical circulator; OC, optical coupler; OI, optical isolator; VA, variable attenuator.

To complicate the modulator and further suppress the TDS, an additional delayed optical feedback loop is added to SL2.

The well-known Lang-Kobayashi rate equations are adopted and modified to model the SLs in this system, which are described as[27–29]

$$\dot{E}_s(t) = \frac{1}{2}(1+i\alpha)\left(G-\frac{1}{\tau_p}\right)E_s(t)+k_sE_s(t-\tau_s)\exp(-i\omega_s\tau_s) +\sigma_sE_m(t-T_s)\exp(-i\omega_mT_s+i\Delta\omega_{sm}t)+\sqrt{2\beta N_s}\chi_s, \tag{1}$$

$$\dot{N}_s(t) = \frac{I}{q}-\frac{1}{\tau_e}N_s(t)-G_s|E_s(t)|^2, \tag{2}$$

where the subscripts s, m $(s,m=1,2,3)$ represent the SL1, SL2, and SL3, E is the complex electric field amplitude, and N is the corresponding carrier number. $G_s(t)=g(N_s(t)-N_0)/(1+\varepsilon|E_s(t)|^2)$ is the optical gain. For the terms on the right-hand side of Eq. (1), the second term represents the optical feedback and only exists for SL2 $(s=2)$, the third term denotes the aforementioned unidirectional injection, and the last term corresponds to the spontaneous emission noise which is modeled by a white gaussian noise χ with zero mean and unity variance. $\beta=10^3$ is the spontaneous emission rate. $k_s(\tau_s)$ is the strength (time delay) of feedback. $\sigma_m(T_s)$ is the strength (flight time) of injection. $\omega=1.216\times10^{15}$ rad/s is the central angular frequency. The frequency detuning between SL1 and SL2, and SL2 and SL3 are defined as $\Delta f_1=\Delta\omega_{12}/2\pi$, $\Delta f_2=\Delta\omega_{23}/2\pi$, respectively, where $\Delta\omega_{sm}=\omega_m-\omega_s$. Here, the operation current I is set as $I=1.5I_{\rm th}$, and the intrinsic parameters of all lasers used in the simulation are assumed to be identical and defined in Table 1.

To identify the TDS of the chaotic signal, the ACF and DMI are adopted, which are defined as

$$P_S(\Delta t)=\frac{\langle(S(t+\Delta t)-\langle S(t)\rangle)(S(t)-\langle S(t)\rangle)\rangle}{(\langle S(t)-\langle S(t)\rangle\rangle^2\langle S(t+\Delta t)-\langle S(t)\rangle\rangle^2)^{1/2}}, \tag{3}$$

Table 1. Intrinsic Parameter Values for the Lasers

Typography	Symbol	Values
Line width enhancement factor	α	5
Photon lifetime	τ_p	2 ps
Carrier lifetime	τ_e	2 ns
Differential gain coefficient	g	1.5×10^{-8} ps^{-1}
Threshold current	$I_{\rm th}$	14.7 mA
Gain saturation factor	ε	5×10^{-7}
Transparent carrier number	N_0	1.5×10^8

$$\zeta_S(\Delta t)=\sum_{S(t),S(t+\Delta t)}p[S(t),S(t+\Delta t)]\log\frac{p[S(t),S(t+\Delta t)]}{p[S(t)]\cdot p[S(t+\Delta t)]}, \tag{4}$$

where $S(t)$ represents either the intensity time-series $I(t)=|E(t)|^2$ or the phase time-series $\varphi(t)=\mathrm{Arg}[E(t)]$, and $\langle\cdot\rangle$ denotes the time average. $p[S(t)]$ is the probability distribution function of $S(t)$, whereas $p[S(t),S(t+\Delta t)]$ is the joint probability distribution function.

In Fig. 2(a), the dynamic behaviors of the chaos generator SL1 in the laser ring configuration are demonstrated. Here, in our simulation, the injection delays in the laser ring are set as $T_1=0.7$ ns, $T_2=1$ ns, and $T_3=1.3$ ns, respectively, and the injection strengths between the adjacent lasers in the ring are set identically. For the purpose of comparison, the bifurcation diagram of the ECSL with conventional optical feedback (COF) in which the time delay τ_f is equal to the total external round trip time of SL1 $(\tau_f=T_1+T_2+T_3)$ is given in Fig. 2(b). It implies that an identical time delay is embedded in the two systems. As shown in Fig. 2, similar to the bifurcation phenomena in the ECSL with COF, the laser ring begins to present chaotic dynamics with the raise of the injection strength.

Figure 3 presents the ACF and DMI computed from the intensity and phase time-series in the ECSL with COF and SL1. Considering that the injection strengths in the laser ring are equal to the feedback strength of the ECSL with COF, the laser ring structure can be regarded as a variation of the ECSL with COF by replacing the COF with a nonlinear modulation optical feedback. As shown in the first two rows of Fig. 3, due to the nonlinear modulation of SL2 and SL3 on the feedback signal of SL1, the TDS of the chaos in SL1 is suppressed with regard to that of the ECSL with COF, especially when the TDS observed by the ACF in the phase space is almost eliminated, which is qualitatively in line with the results in Ref. [25]. Nevertheless, it should be acknowledged that the size of the TDS remains detectable under this condition. That is, the TDS suppression is to some extent not well achieved. To further suppress the TDS, a delayed feedback loop with time delay $\tau_2=2$ ns and a feedback strength $k_2=30$ ns^{-1} is added to the SL2. It is clear that the TDS embedded in both the intensity and phase time-series is effectively eliminated

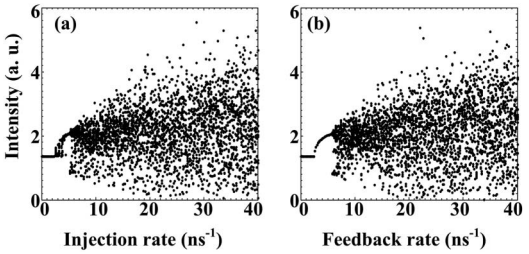

Fig. 2. Bifurcation diagrams for (a) the proposed laser ring with $T_1=0.7$ ns, $T_2=1$ ns, $T_3=1.3$ ns, $\Delta f_1=\Delta f_2=0$ GHz, and $k_2=0$ ns^{-1}, and (b) the ECSL subject to COF.

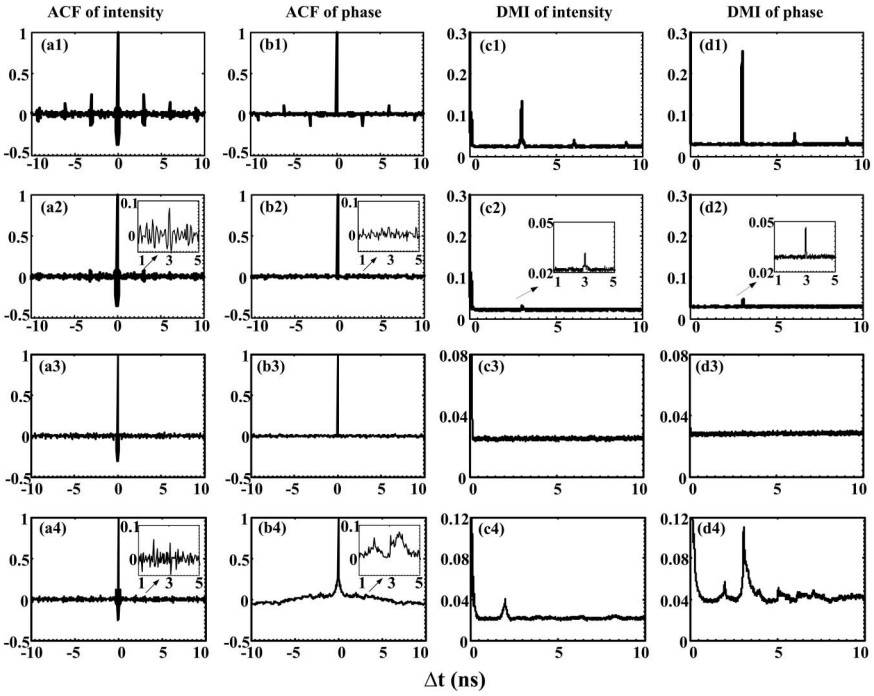

Fig. 3. ACF (the first and second columns) and DMI (the third and fourth columns) computed from the intensity and phase time-series of chaos in different systems, respectively. The first row is for the ECSL with COF ($k_f = 20$ ns^{-1}, $\tau_f = 3$ ns), the second row is for the laser ring without a feedback loop in SL2, the third row is for the laser ring with a moderate feedback loop in SL2 ($k_2 = 30$ ns^{-1}, $\tau_2 = 2$ ns), and the fourth row is for a feedback strength enhanced case ($k_2 = 60$ ns^{-1}). Parameters for the injection in the laser ring are set as $\sigma_1 = \sigma_2 = \sigma_3 = 20$ ns^{-1}, $T_1 = 0.7$ ns, $T_2 = 1$ ns, $T_3 = 1.3$ ns, and $\Delta f_1 = \Delta f_2 = 0$ GHz.

[Figs. 3(a3)–3(d3)], because the introduced feedback loop in SL2 can enhance the complexity and power of the nonlinear modulator. When we enhance the strength of feedback in the SL2 to 60 ns^{-1}, the performance of the TDS suppression becomes worse again [see Figs. 3(a4)–3(d4)], and this is because an overtop feedback in SL2 would break the balance between the injection and feedback in the nonlinear modulator and introduce a new TDS in the chaos of SL2 (not shown here), which can be transferred to SL1. Moreover, we also investigate the TDS characteristics with PE, the results (not shown here) are similar to those of the ACF and DMI.

Figure 4 shows the evolution of TDS in SL1 evaluated by the ACF and DMI (the TDS is numerically denoted as the maximum value of the peaks and valleys in the ACF and DMI with respect to the time average) in the space of the injection strengths and feedback strength in SL2. When the feedback strength in SL2 is relatively weak, it is difficult to further suppress the TDS for its limited role in the nonlinear modulation. When the feedback strength is moderate, the TDS of SL1 can be efficiently suppressed. Whereas when the feedback strength is very strong, the nonlinear modulation is mainly determined by the feedback of SL2, and then new maximum peaks or valleys for the ACF and DMI appear at $\Delta t = 2$ ns which is equal to the feedback delay of SL2. Over all, there is a large region in which the TDS embedded in the intensity and phase time-series of the chaos can be well suppressed.

Next, the influence of the time delay of feedback in SL2 on the TDS suppression is investigated. As shown in Fig. 5, the TDS suppression is non-sensitive to the time delay of feedback in SL2 once the injection and feedback strength in fixed. In addition, the time delay of feedback in SL2 is suggested to not equal to the total time delay of the system.

A two dimensional map of the TDS stemming from the intensity and phase time-series in the parameter space of

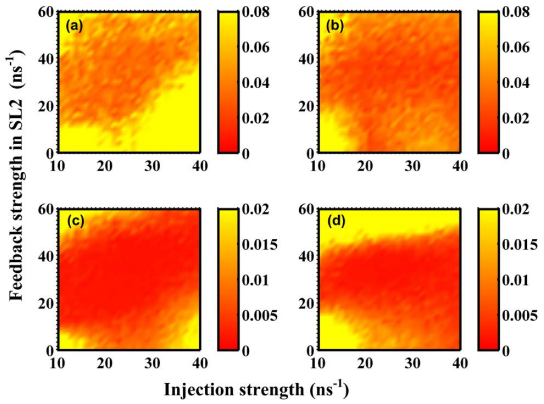

Fig. 4. TDS size as a function of the injection strengths and feedback strength in SL2. (a) and (b) present the TDS observed by the ACF from the intensity and phase time-series, respectively, and (c) and (d) show the TDS identified by the DMI from the intensity and phase time-series, respectively; $\Delta f_1 = \Delta f_2 = 0$ GHz.

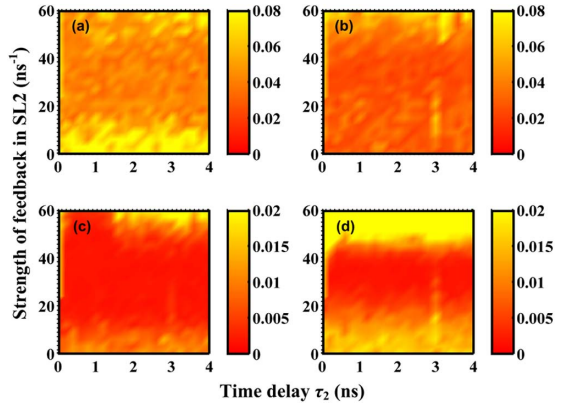

Fig. 5. TDS size as a function of the feedback strength and time delay in SL2 with $\sigma_1 = \sigma_2 = \sigma_3 = 20$ ns^{-1} and $\Delta f_1 = \Delta f_2 = 0$ GHz. (a) and (b) present the TDS observed by the ACF from the intensity and phase time-series, respectively, and (c) and (d) show the TDS identified by the DMI from the intensity and phase time-series, respectively.

frequency detuning Δf_1 and Δf_2 is presented in Fig. 6. It is apparent that the ACF and DMI indicate similar areas in the frequency detuning space for the TDS suppression, respectively. Also, the TDS suppression computed by the ACF and DMI from the phase time-series has a smaller area with respect to that in the intensity time-series. After all, it should be acknowledged that the TDS concealment in our system is robust to the frequency detuning, and efficient TDS suppression can be achieved in a large range of frequency detuning.

This Letter proposes a more powerful scheme for TDS concealment in the chaotic SLs by introducing nonlinear modulated feedback in the external cavity of SLs. In this scheme, three SLs are unidirectionally coupled to form a ring in which one SL works as the chaos generator, and the other two jointly play the role of nonlinear modulator. The TDS concealment of the chaotic signal in the chaos

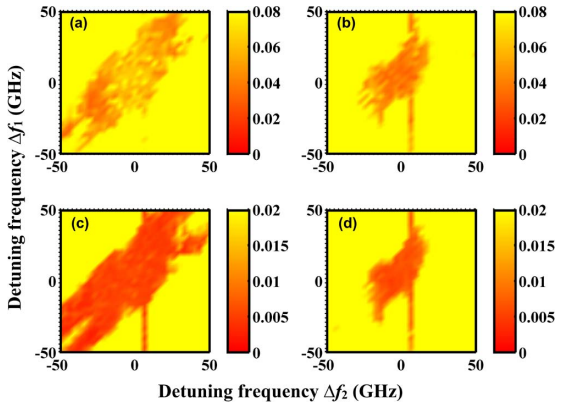

Fig. 6. Evolution of the TDS size in the detuning frequency space with $\sigma_1 = \sigma_2 = \sigma_3 = 20$ ns^{-1}, and $k_2 = 30$ ns^{-1}. (a) and (b) present the TDS observed by the ACF from the intensity and phase time-series, respectively, and (c) and (d) show the TDS identified by the DMI from the intensity and phase time-series, respectively.

generator is thoroughly investigated via the calculations of the ACF and DMI. The numerical results indicate that, with respect to the laser ring without a feedback loop in the nonlinear modulator, the one with a delayed feedback loop obviously shows a better TDS suppression property. Moreover, the TDS suppression can be achieved in a wide range of operation parameters and frequency detuning. In a word, although it is a more complex system with respect to a single ECSL, the proposed scheme could be easy to implement in photonic integrated circuits to generate chaos with the TDS eliminated; therefore it has great potential applications in the chaos-based secure communication and high speed RBGs.

This work was supported in part by the National Science Foundation of China (NSFC) (Nos. 61301156 and 61471087), the Specialized Research Fund for the Doctoral Program of Higher Education of China (No. 20130185120007), and the Fundamental Research Funds for the Central Universities (No. ZYGX2013J001).

References

1. T. Matsuura, A. Uchida, and S. Yoshimori, Opt. Lett. **29**, 2731 (2004).
2. A. Argyris, D. Syvridis, L. Larger, V. Annovazzi-Lodi, P. Colet, I. Fischer, J. Garcla-Ojalvo, C. R. Mirasso, L. Pesquera, and K. A. Shore, Nature **438**, 343 (2005).
3. Y. Hong, M. W. Lee, J. Paul, P. S. Spencer, and K. A. Shore, IEEE J. Lightwave Technol. **27**, 5099 (2009).
4. N. Jiang, C. Zhang, and K. Qiu, Opt. Lett. **37**, 4501 (2012).
5. A. Uchida, K. Amano, M. Inoue, K. Hirano, S. Naito, H. Someya, I. Oowada, T. Kurashige, M. Shiki, S. Yoshimori, K. Yoshimura, and P. Davis, Nat. Photon. **2**, 728 (2008).
6. I. Kanter, Y. Aviad, I. Reidler, E. Cohen, and M. Rosenbluh, Nat. Photon. **4**, 58 (2010).
7. A. Wang, P. Li, J. Zhang, J. Zhang, L. Li, and Y. Wang, Opt. Express **21**, 20452 (2014).
8. R. Sakuraba, K. Iwakawa, K. Kanno, and A. Uchida, Opt. Express **23**, 1470 (2015).
9. F. Y. Lin and J. M. Liu, IEEE J. Quantum Electron. **40**, 682 (2004).
10. W. T. Wu, Y. H. Liao, and F. Y. Lin, Opt. Express **18**, 26155 (2010).
11. Y. Wang, B. Wang, and A. Wang, IEEE Photon. Technol. Lett. **20**, 1636 (2008).
12. R. Hegger, M. J. Bünner, H. Kantz, and A. Giaquinta, Phys. Rev. Lett. **81**, 558 (1998).
13. Y. Wu, Y. Wang, P. Li, and A. Wang, IEEE J. Quantum Electron. **48**, 1371 (2012).
14. D. Rontani, A. Locquet, M. Sciamanna, D. S. Citrin, and S. Ortin, IEEE J. Quantum Electron. **45**, 879 (2009).
15. L. Zunino, M. C. Soriano, I. Fischer, O. A. Rosso, and C. R. Mirasso, Phys. Rev. E **82**, 046212 (2010).
16. R. M. Nguimdo, M. C. Soriano, and P. Colet, Opt. Lett. **36**, 4332 (2011).
17. D. Rontani, A. Locquet, M. Sciamanna, and D. S. Citrin, Opt. Lett. **32**, 2960 (2007).
18. J. Wu, G. Xia, and Z. Wu, Opt. Express **17**, 20124 (2009).
19. R. M. Nguimdo, G. Verschaffelt, J. Danckaert, and G. Van der Sande, Opt. Lett. **37**, 2541 (2012).
20. S. Li, Q. Liu, and S. Chan, IEEE Photon. J. **4**, 1930 (2012).
21. S. Priyadarshi, Y. Hong, I. Pierce, and K. A. Shore, IEEE J. Sel. Top. Quantum Electron. **19**, 1700707 (2013).

22. S. Xiang, W. Pan, A. Wen, N. Li, L. Zhang, L. Shang, and H. Zhang, IEEE Photon. Technol. Lett. **25**, 1398 (2013).
23. X. Dou, C. Wu, X. Chen, H. Yin, Q. Zhao, Y. Hao, and N. Zhao, Chin. Opt. Lett. **12**, S10610 (2014).
24. M. Cheng, X. Gao, L. Deng, L. Liu, Y. Deng, S. Fu, M. Zhang, and D. Liu, IEEE Photon. Technol. Lett. **27**, 1030 (2015).
25. L. Yang, W. Pan, L. Yan, B. Luo, P. Mu, and N. Li, Chin. Opt. Lett. **13**, 041403 (2015).
26. A. Wang, Y. Yang, B. Wang, B. Zhang, L. Li, and Y. Wang, Opt. Express **21**, 8701 (2013).
27. R. Lang and K. Kobayashi, IEEE J. Quantum Electron. **16**, 347 (1980).
28. R. Vicente, C. R. Mirasso, and I. Fischer, Opt. Lett. **32**, 403 (2007).
29. C. Xue, N. Jiang, K. Qiu, and Y. Lv, Opt. Express **23**, 14510 (2015).